Electronic Supporting Information

Activating Nickel Foam with Trace Titanium Oxide for Enhanced Water Oxidation

1. Experimental Section:

Chemicals and reagents. Butyl titanate (98%, Sinopharm Chemical Reagent Co., Ltd), KOH (99.99%, Aladdin), Ni foam (99.9%, Kunshan Guangjiayuan New Material Co., Ltd), HF solution (40%, Macklin), ethanol (Sinopharm Chemical Reagent Co., Ltd). Ultrapure water was used in this work. Ni foam (NF) was used after sonication in acetone, ethanol, and 0.1 M HCl solution for 15 min, respectively. Ultrapure water was used.

Synthesis of TiO$_2$ nanosheets. TiO$_2$ nanosheets were synthesized using a modified hydrothermal method.[1] Briefly, 25 mL butyl titanate was dropped into 15 mL HF solution (24 wt.%) with stirring. After stirring for 30 min, the solution was transferred into a 50 mL hydrothermal autoclave reactor, and heated at 180 °C for 24 h. The white powder was obtained by washing with ethanol and water for three times, respectively, and finally dried at 60 °C overnight.

Synthesis of TiO$_2$@NF (prepared Ti-Ni). In a typical experiment, 1 mg TiO$_2$ nanosheets were dispersed in 1 mL water with sonication. 15 μg cm^{-2} of ink was dropped on freshly washed NF and dried under IR lamp. To anchoring TiO$_2$ nanosheets on NF, they were heated in the air at 400 °C for 5 h. The bare NF that heated under the same program was denoted as the annealed NF.

Synthesis of activated Ti-Ni. Activated Ti-Ni was derived from electrochemical activation of prepared Ti-Ni in an alkaline flow cell for carbon dioxide reduction, in which prepared Ti-Ni anode shared the same geometric size as cathode and HgO was the reference electrode. The catholyte and anolyte were 1 M KOH and was recirculating with the flow

rate of 5 mL min^{-1}. Activated Ti-Ni was obtained after the three-electrode electrolysis, which was conducted at a series of constant current densities of 50, 100, 150, 200, and 250 mA cm^{-2}.

Characterization. Scanning electron microscope (SEM) image was obtained using a field emission scanning electron microscope (S 4800, Hitachi). X-ray power diffraction (XRD) pattern of TiO_2 nanosheets was recorded on a X'Pert Pro (PANalytical). The chemical valence of the materials was characterized by X-ray photoelectron spectroscopy (Axis Supra, Shimadzu). The specific correction was done by employing the C 1s binding energy of 284.8 eV. Raman spectra were collected by a Raman spectrometer (LabRAM Aramis, Horiba Jobin Yvon S.A.S.).

Electrochemical measurements.

Electrocatalytic water oxidation activity and durability were conducted by an electrochemical work station (CHI 660E) with the three-electrode system in a single reactor. The counter electrode is a Pt plate (2 cm × 2 cm), and the reference electrode was HgO (1 M KOH). The water oxidation LSV was carried out at a scan rate of 5 mV s^{-1}. The double layer capacitance (C_{dl}) was evaluated in the range of non-Faradaic zone. And the electrochemical active surface area (ECSA) values were calculated from the measured double layer capacitance divided by the specific capacitance of an atomically smooth material (C_{dl}', ~40 μF cm^{-2}) in 1.0 M KOH: ECSA = $C_{dl} \div C_{dl}' \times S$, where S is the actual surface area of the electrode.[2,3] Electrochemical impedance spectroscopy (EIS) was conducted in the frequency range from 0.1 Hz to 1 MHz at 0.6 V vs HgO. The stability test was conducted

at the constant current density of 10 mA cm^{-2}. All the potentials reported in the work are with iR correction unless otherwise specified, which are given versus reversible hydrogen electrode (RHE) according to $E_{RHE} = E_{HgO} + 0.098$ V$+ 0.0591 \times$ pH. The electrolyte was 1 M KOH, of which the experimental pH was 13.5 according to the reference.[4] To comparison, the same loading mass of IrO_2 nanoparticles was anchored on NF.

In-situ Raman spectroscopy.

All *in-situ* Raman spectroscopy tests were conducted at a Raman spectrometer (LabRAM Aramis, Horiba Jobin Yvon S.A.S.). Laser excitation was conducted at 532 nm. Prior to use, the Raman shift range was calibrated using the 520.6 ± 0.5 cm^{-1} peak of silicon. The working electrode was contacted with a Pt electrode holder and then assembled to the custom-made electrochemical cell.

2. Supporting experimental results:

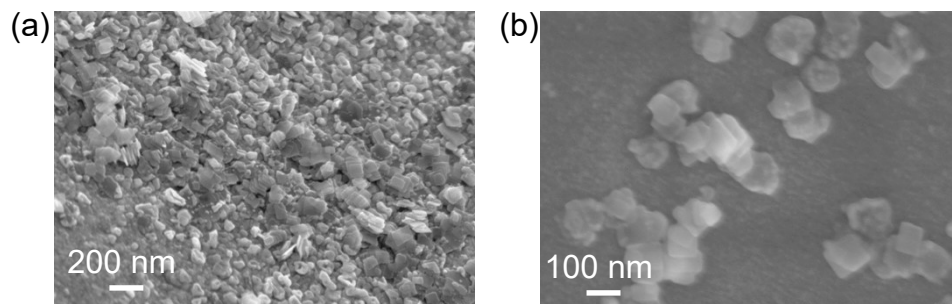Figure S1. (a) SEM and (b) XRD of TiO$_2$ nanosheets.
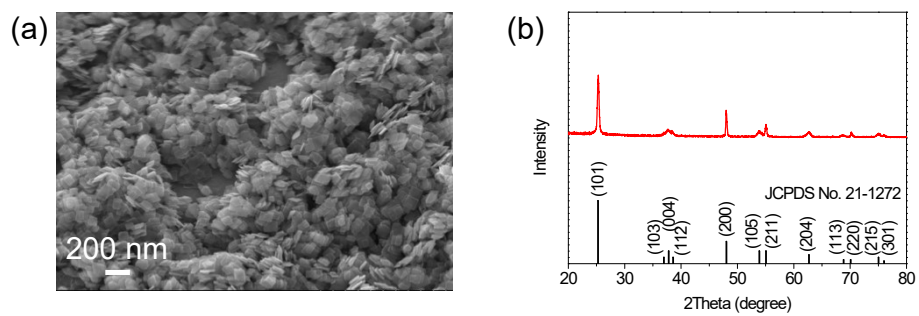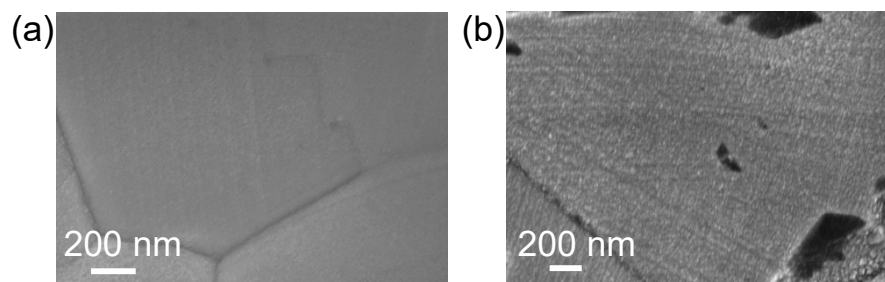
Figure S2. SEM images of prepared Ti-Ni.

Figure S3. SEM image of (a) bare NF and (b) annealed NF.

The rough surface of prepared Ti-Ni in Figure S2 came from the surface change of NF itself during heat treatment. In this case, bare NF sample for Figure S3(a) was washed with alcohols only.
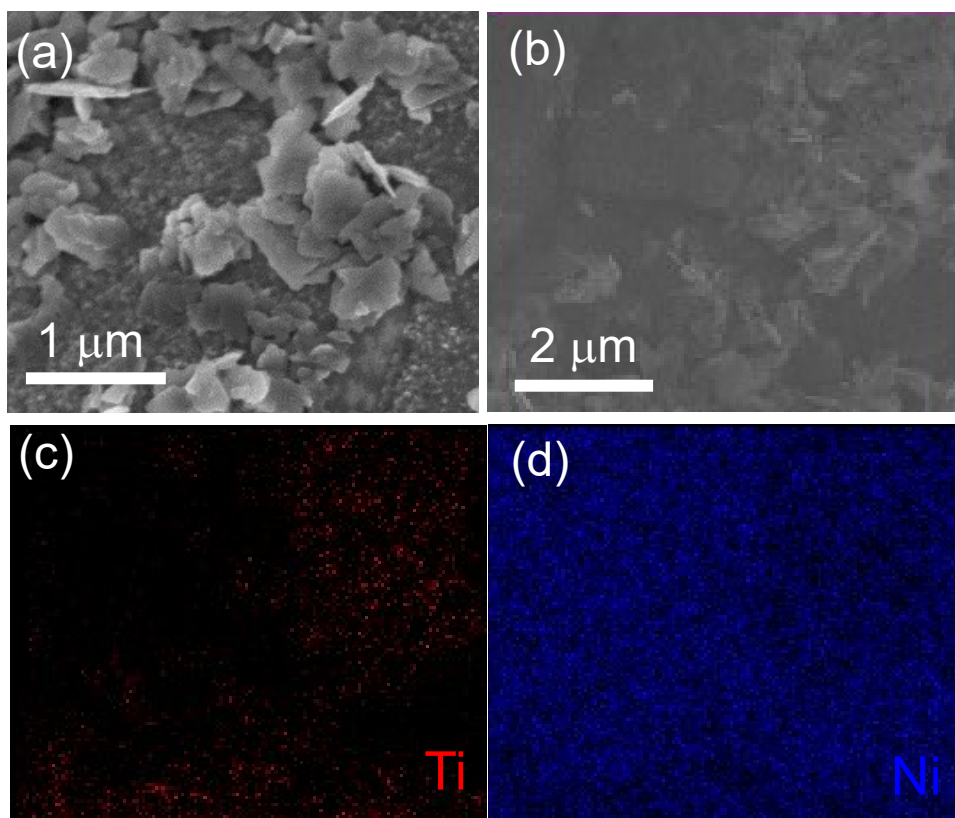
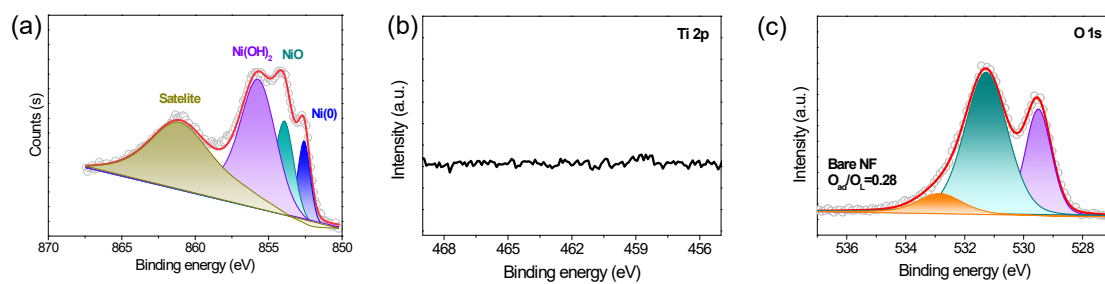Figure S4. (a and b) SEM images and (c and d) corresponding mapping of the activated

Ti-Ni.

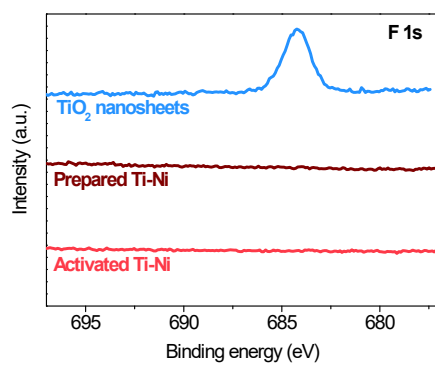Figure S5. XPS spectra of bare NF. (a) Ni 2p, (b) Ti 2p, and (c) O 1s.

Figure S6. F 1s XPS spectra for TiO_2 nanosheets, prepared Ti-Ni, and activated Ti-Ni.
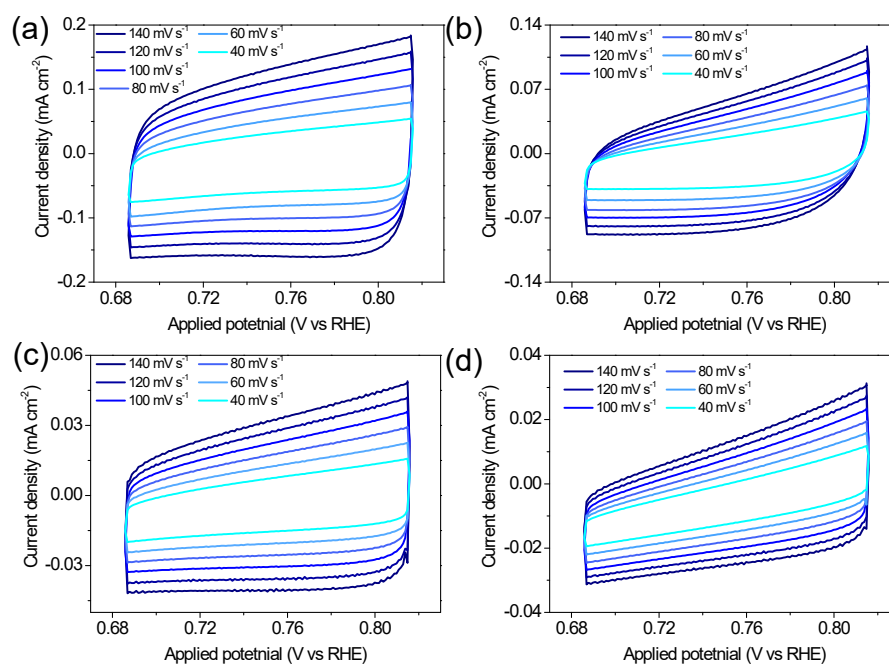
Figure S7. Cyclic voltammetry plots of (a) activated Ti-Ni, (b) IrO_2, (c) prepared Ti-Ni, and

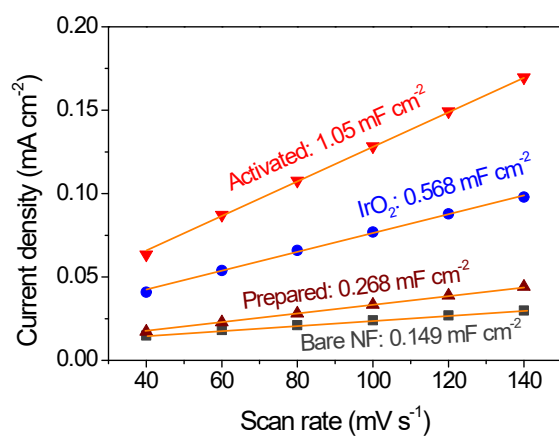(d) bare NF with a series of scan rates in the non-Faradaic region.

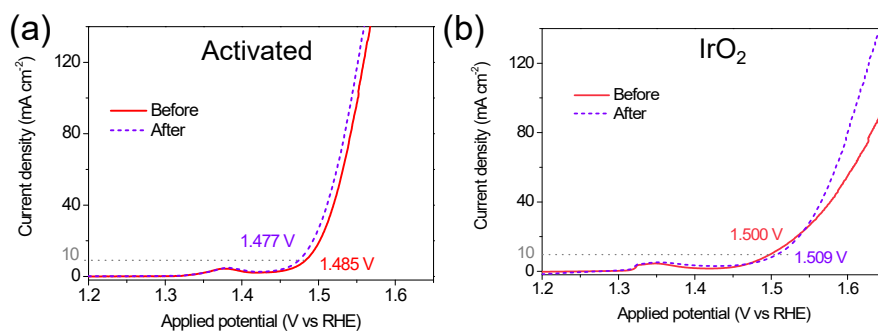Figure S8. Linear fitting of capacitive currents against CV scan rates.

Figure S9. LSV plots of (a) activated Ti-Ni and (b) IrO_2 before and after stability test under 10 mA cm^{-2} for 24 h.
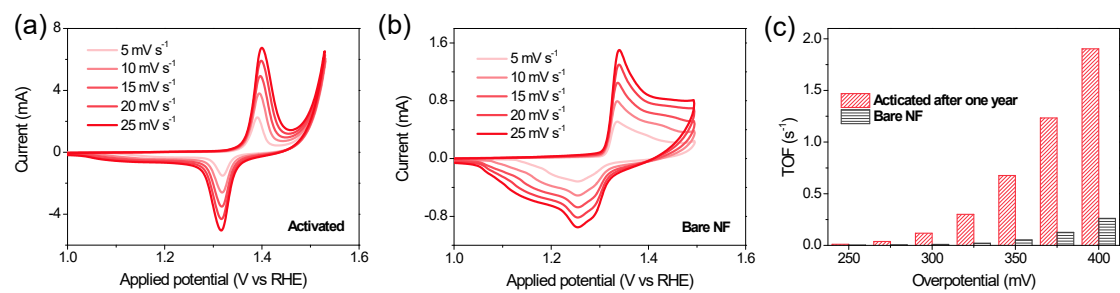
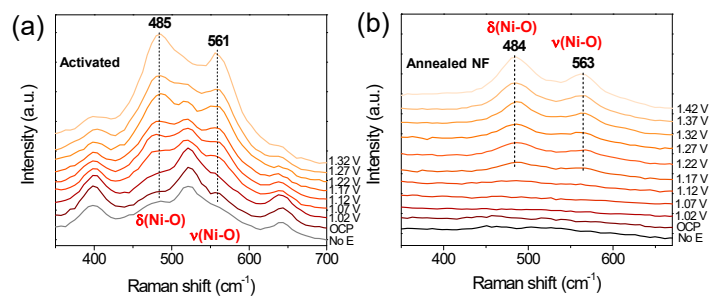Figure S10. CV plots of (a) activated Ti-Ni and (b) bare NF. (c) Resulting TOF.

Figure S11. Local magnified Raman spectra in the range of 350-700 cm^{-1} for the Ni region. (a) Activated Ti-Ni, (b) Annealed NF. OCP: open circuit potential was applied. No E: no potential was applied.
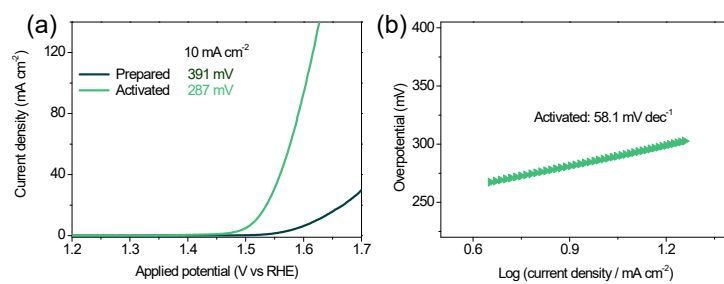
Figure S12. OER performance on prepared and activated Ti-Ni synthesized with commercial P25 nanoparticles instead of TiO_2 nanosheets.

3. Table S1. Recent TiO_2 contained electrocatalysts for alkaline water oxidation.

Catalyst	Mass loading (mg cm^{-2})	Electrolyte	η_{10} (mV)	η_{100} (mV)	$\eta_{1\text{-ECSA}}$ (mV)	Tafel slope (mV dec^{-1})	Retained / durability test	Ref
Activated Ti-Ni	0.015	1.0 mol L^{-1} KOH	256	337	282	59	100% / 24 h 99.8% / 100 h	This work
NiO/TiO$_2$	0.34	1.0 mol L^{-1} KOH	320	NM	NM	52	NM / 10 h	*J. Am. Chem. Soc.* **2016**, 138, 6517.[5]
O$_V$-TiO$_2$	~0.102[a]	1.0 mol L^{-1} KOH	600	NM	NM	51	~96%[a] / 36 h	*J. Am. Chem. Soc.* **2016**, 138, 9978.[6]
Rutile-anatase TiO$_2$/RGO	0.25	1.0 mol L^{-1} KOH	283	~372[a]	NM	94	~98%[a]/ 10 h	ChemNanoMat, **2018**, 4, 1133-1139.[7]
Co$_3$O$_4$(x)/Ism-TiO$_2$	0.8	1.0 mol L^{-1} KOH	348	~570[a]	NM	54	92% / 9 h	*Catalysts* **2019**, 9, 836.[8]
Co-TiO$_2$	0.21 (12% Co)	1.0 mol L^{-1} KOH	332	396	~310[a]	72	99% / 10 h	*Nature Catalysis* **2020**, 4, 36.[9]
Fe-UTN	~0.34[a] (11.74% Fe)	1.0 mol L^{-1} KOH	270	376	NM	~36.5[a]	92.3% / 10 h	*Angew. Chem. Int. Ed.* **2020**, *59*, 2313-2317.[10]
Defective RuO$_2$/TiO$_2$	1.19	1.0 mol L^{-1} KOH	296	358	NM	46.6	20 h	*Chem. Eng. J.* **2022**, *431*, 134072.[11]

Note: [a] calculated from the data from the corresponding literature.

REFERENCES

(1) Liu, C.; Zhang, A.-Y.; Si, Y.; Pei, D.-N.; Yu, H.-Q., Photochemical Anti-Fouling Approach for Electrochemical Pollutant Degradation on Facet-Tailored TiO_2 Single Crystals. *Environ. Sci. Technol.* **2017**, *51* (19), 11326-11335.

(2) Song, Z.; Wang, K.; Sun, Q.; Zhang, L.; Li, J.; Li, D.; Sze, P.-W.; Liang, Y.; Sun, X.; Fu, X.-Z.; Luo, J.-L., High-Performance Ammonium Cobalt Phosphate Nanosheet Electrocatalyst for Alkaline Saline Water Oxidation. *Adv. Sci.* **2021**, *8* (14), 2100498.

(3) Liu, P.; Chen, B.; Liang, C.; Yao, W.; Cui, Y.; Hu, S.; Zou, P.; Zhang, H.; Fan, H. J.; Yang, C., Tip-Enhanced Electric Field: A New Mechanism Promoting Mass Transfer in Oxygen Evolution Reactions. *Adv. Mater.* **2021**, *33* (9), 2007377.

(4) Görlin, M.; Halldin Stenlid, J.; Koroidov, S.; Wang, H.-Y.; Börner, M.; Shipilin, M.; Kalinko, A.; Murzin, V.; Safonova, O. V.; Nachtegaal, M.; Uheida, A.; Dutta, J.; Bauer, M.; Nilsson, A.; Diaz-Morales, O., Key Activity Descriptors of Nickel-Iron Oxygen Evolution Electrocatalysts in the Presence of Alkali Metal Cations. *Nat. Commun.* **2020**, *11* (1), 6181.

(5) Zhao, Y.; Jia, X.; Chen, G.; Shang, L.; Waterhouse, G. I.; Wu, L. Z.; Tung, C. H.; O'Hare, D.; Zhang, T., Ultrafine NiO Nanosheets Stabilized by TiO_2 from Monolayer NiTi-LDH Precursors: An Active Water Oxidation Electrocatalyst. *J. Am. Chem. Soc.* **2016**, *138* (20), 6517-6524.

(6) Tao, H. B.; Fang, L. W.; Chen, J. Z.; Yang, H. B.; Gao, J. J.; Miao, J. W.; Chen, S. L.; Liu, B., Identification of Surface Reactivity Descriptor for Transition Metal Oxides in Oxygen Evolution Reaction. *J. Am. Chem. Soc.* **2016**, *138* (31), 9978-9985.

(7) Hu, Y. W.; Ding, T.; Zhang, K. L.; Li, B.; Zhu, B. C.; Tang, K. B., Component-Tunable Rutile-Anatase TiO_2/Reduced Graphene Oxide Nanocomposites for Enhancement of Electrocatalytic Oxygen Evolution. *Chemnanomat* **2018**, *4* (11), 1133-1139.

(8) Amer, M. S.; Ghanem, M. A.; Arunachalam, P.; Al-Mayouf, A. M.; Hadadi, S. M., Bifunctional Electrocatalyst of Low-Symmetry Mesoporous Titanium Dioxide Modified with Cobalt Oxide for Oxygen Evolution and Reduction Reactions. *Catalysts* **2019**, *9* (10), 836.

(9) Liu, C.; Qian, J.; Ye, Y.; Zhou, H.; Sun, C.-J.; Sheehan, C.; Zhang, Z.; Wan, G.; Liu, Y.-S.; Guo, J.; Li, S.; Shin, H.; Hwang, S.; Gunnoe, T. B.; Goddard, W. A.; Zhang, S., Oxygen Evolution Reaction over Catalytic Single-Site Co in a Well-Defined Brookite TiO_2 Nanorod Surface. *Nat. Catal.* **2020**, *4* (1), 36-45.

(10) Shen, G. Q.; Zhang, R. R.; Pan, L.; Hou, F.; Zhao, Y. J.; Shen, Z. Y.; Mi, W. B.; Shi, C. X.; Wang, Q. F.; Zhang, X. W.; Zou, J. J., Regulating the Spin State of Fe^{III} by Atomically Anchoring on Ultrathin Titanium Dioxide for Efficient Oxygen Evolution Electrocatalysis. *Angew. Chem. Int. Ed.* **2020**, *59* (6), 2313-2317.

(11) Yu, J. Y.; Wang, X. D.; Huang, X. W.; Cao, J. Y.; Huo, Q. H.; Mi, L. R.; Yang, H. P.; Hu, Q.; He, C. X., Confining Ultrafine Ru Clusters into TiO_2 Lattice Frameworks to Yield Efficient and Ultrastable Electrocatalysts Towards Practical Hydrogen Evolution. *Chem. Eng. J.* **2022**, *446* 137248.